Article

Structure and Mechanical Properties of Milled and 3D Printed Ti-6Al-4V Alloys for Subtractive and Additive CAD/CAM Manufacturing in Dentistry

Sabina Cherneva *, Vladimir Petrunov, Vladimir Petkov, Vladimir Bogdanov, Silviya Simeonova

Posted Date: 10 October 2023

doi: 10.20944/preprints202310.0629.v1

Keywords: titanium alloys; milling; selective laser melting; mechanical properties; surface structure

Article

Structure and Mechanical Properties of Milled and 3D Printed Ti-6Al-4V Alloys for Subtractive and Additive CAD/CAM Manufacturing in Dentistry

Sabina Cherneva [1,*], Vladimir Petrunov [2], Vladimir Petkov [3], Vladimir Bogdanov [2] and Silviya Simeonova [4]

[1] Institute of Mechanics, Bulgarian Academy of Sciences, Acad. G. Bontchev St., bl. 4, 1113 Sofia, Bulgaria; sabina_cherneva@yahoo.com

[2] Faculty of Dental Medicine, Medical University of Sofia, St. Georgi Sofiiski Blvd., 1431 Sofia, Bulgaria; dr.petrunov@gmail.com, vladbogdanov@yahoo.com

[3] Institute of Metal Science, Equipment and Technologies with Hydro- and Aerodynamics Centre "Acad. A. Balevski", Bulgarian Academy of Sciences, 67 Shipchenski prohod Street, 1113 Sofia, Bulgaria; vladimir2pe@yahoo.com.

[4] Faculty of Chemistry and Pharmacy, Sofia University, 1 James Bourchier Blvd., 1164 Sofia, Bulgaria; fhsss@chem.uni-sofia.bg.

* Correspondence: sabina_cherneva@yahoo.com; Tel.: +359-2-979-67-51

Abstract: The mechanical properties, structure, and morphology of milled and 3D printed Ti-6Al-4V alloys produced by selective laser melting were investigated in this study. The mechanical properties were investigated by means of nanoindentation, a tensile test, and a three-point bending test. The Atomic Force Microscope (AFM) was used to study the surface topography and roughness of both titanium alloys. The surface structure and phase analysis were studied by a scanning electron microscope (SEM) and through powder X-ray diffraction (XRD). The results from the nanoindentation experiments showed that the 3D-printed sample has higher indentation hardness and modulus than the milled one. The AFM observation of the surface topography of the samples showed that the milled sample has a higher roughness than the 3D-printed one. The tensile test results showed that the 3D printed sample by means of Selective Laser Melting (SLM) technology has about 26% higher tensile strength and smaller elongation than the milled one. The 3-point bending test revealed that the 3D printed Ti-6Al-4V sample has higher flexural strength than the milled one. It was found that the 3D-printed sample has a smaller crystal size than the milled one, which, according to the Hall-Petch relationship, leads to its higher indentation hardness.

Keywords: titanium alloys; milling; selective laser melting; mechanical properties; surface structure

1. Introduction

In recent years, we have been witnessing an era of digitization in dental medicine. With the entry into daily practice of methods such as intraoral scanning, digital imaging diagnostics, and the planning and manufacturing of structures and orthodontic appliances through CAD/CAM methods, the classic working protocol is being replaced by a digital one. Today, CAD/CAM methods are routinely used in almost all areas of dentistry for the fabrication of prosthetic structures [1,2], orthodontic appliances [3], and in implantology for the production of surgical guides and individual abutments [4,5].

CAD/CAM methods are related to the planning of constructions using specialized software, after which they are made by machines with digital program control through methods of subtractive production (milling or additive production) and 3D printing. Each one of these methods has its own technological advantages and disadvantages. Milling is the removal of material from a monolithic block using a specialized multi-axis milling machine. The accuracy and quality of the workpiece in this method are determined by the number of milling axes [6], the smallest cutter size [7], adequate

 doi:10.20944/preprints202310.0629.v1

cooling, and the absence of vibration during milling, which depends on the correct planning of the supports [8].

One serious disadvantage of this method is the large amount of waste material that is milled. This increases the cost of the final product. Additive manufacturing is a method in which an object is built by fusing material, accomplished by sequentially bonding layer after layer [9]. The main advantages of this production method are that it allows the production of objects with a very complex shape, there is no need to change depreciable consumables such as cutters [10], and it is economical in terms of the material used, which is essential when it comes to expensive raw materials such as Ti.

Another disadvantage of this method is the expensive equipment and sensitive technology, which, if not properly performed, can spoil the final result. In modern dentistry, more and more attention is paid to the biocompatibility of the materials used. Another important point to consider when choosing a material is its mechanical properties. Ti–6Al–4V or Ti G5 is an alloy widely used in dentistry. It has excellent biocompatibility [11,12] and good mechanical properties [13]. In our practice, we use Ti G5 to fabricate long-term or lifelong orthodontic retainers (Figure 1) made by CAD/CAM methods.

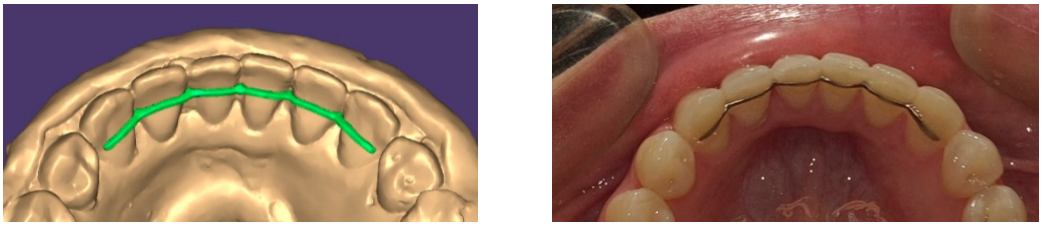

(**a**) (**b**)

Figure 1. (**a**) CAD/CAM planned orthodontic retainer; (**b**) Intraoral view of the retainer.

The producing method, the surface characteristics, and the added trace elements have significant influence on the mechanical properties of investigated titanium alloys [14]. The aim of the present study is to compare the mechanical properties and surface characteristics of two titanium alloys for subtractive and additive CAD/CAM manufacturing in dental medicine.

2. Materials and Methods

A 3D-printed titanium alloy was produced from metal powder, PowderRange Ti64 (Carpenter Technology Corp.), on a selective laser fusion apparatus, MYSINT100 (SISMA S.p.A.), using a fiber laser source. The manufacturing parameters of the 3D printed titanium alloy are given in Table 1.

Table 1. Manufacturing parameters of the 3D printed Ti–6Al–4V sample.

Manufacturing parameter	Value	Unit
Laser power	140	W
Layer thickness	30	µm
Laser spot	50	µm
Scan speed	125	mm/sec
Hatch spacing	80	µm
Oxygen level	<0.3	%
Build platform heating	200	°C

For the milled Ti, Ti G5 discs (SILADENT Dr. Böhme & Schöps GmbH) were used, and it was milled on a CORiTEC 650i 5-axis milling machine (Imes-icore GmbH). The surface morphology and the elemental composition were studied by a scanning electron microscope (SEM) "HIROX SH-5500P" with an integrated Energy-Dispersive X-Ray Spectroscopy (EDS) system "QUANTAX 100 Advanced"—Bruker. The SEM has an accelerating voltage range of 1–30 kV. The investigation was conducted at 20 kV.

 doi:10.20944/preprints202310.0629.v1

The microstructure of the samples was analysed using a "MIT500" microscope at magnifications up to 1000x and photographed with a DV500 digital camera. Metallographic samples were prepared according to a standard procedure. The microstructure of titanium samples was revealed by immersing them in the following solution: 1 ml HNO_3 + 1ml HF + 48ml H_2O.

An X-ray structural analysis of the investigated alloys was made using the powder X-ray diffraction method. The investigations were done with a Bruker D8 Advance powder X-ray diffractometer. The Bruker DIFFRAC.EVA v4 program and ICDD PDF-2 (2021) comparison database with reference measurements of inorganic compounds were used to determine the qualitative and quantitative phases of analysis. Crystallite size was calculated along a single line using the Scherrer equation and a Bruker Topas v4.2 diffraction profile analysis program.

The surface topography was studied by means of atomic force microscopy (AFM). AFM imaging was performed on the NanoScope V system (Bruker Inc., Germany) operating in tapping mode in air at room temperature. Silicon cantilevers (Tap 300 Al-G, Budget Sensors, Innovative Solutions Ltd., Bulgaria) with a 10 nm-thick aluminum reflex coating were used. The scanning rate was set at 0.5 Hz, and a scanning size of 10 μm × 10 μm and 5 μm × 5 μm was applied. The images were taken in the highest possible resolution mode of the AFM, 512 x 512 pixels in JPEG format using the NanoScope software.

The mechanical properties of both alloys were investigated by means of a tensile test, a three-point bending test, and nanoindentation experiments. The tensile test was made according to the ISO 6892-1:2019 standard, using the electromechanical machine Instron 1185 (UK) at an absolute deformation rate of 0.2 mm/min. The three-point bending test was made according to the ISO 7438:2020 standard using the electromechanical machine Mecmesin 2, 5-i (UK) at a speed of absolute deformation of 1 mm/min.

The nanoindentation experiments were made according to the ISO 14577 standard [15] using a Nanoindenter G200 (KLA Corporation, Milpitas, USA) with a Berkovich tip. The indentation method with five loading-unloading cycles and load control was used in order to check if there were changes in the properties of the samples in depth. The maximum load was 30 gf (~294 mN), the peak hold time at the maximum load was 10s, and the time to load was 15s. Twenty-five indentations of each sample were made at a distance of 50 m between them.

SPSS version 27.0 was used for the statistical analyses (SPSS Inc., Chicago, IL, USA). The Shapiro-Wilk test was performed to check the normality of the continuously measured variables. Since normality was present ($p > 0.10$ for all tests), the results were described with the means and standard deviations (SDs), and the independent samples t-test was used for between-group comparisons. The statistical tests were two-tailed at a Type-I error alpha of 0.05, with p-values < 0.05 being considered significant.

3. Results

3.1. SEM results

SEM studies were performed directly on the surfaces of the titanium disk samples with no mechanical or chemical treatment. The surface structure was photographed at a magnification of x2000 on milled titanium (Figure 2) and on 3D-printed titanium (Figure 3). From Figures 2 and 3, it is evident that the surface of the 3D-printed titanium sample is smoother compared to the milled one.

Preprints (www.preprints.org) | NOT PEER-REVIEWED | Posted: 10 October 2023 doi:10.20944/preprints202310.0629.v1

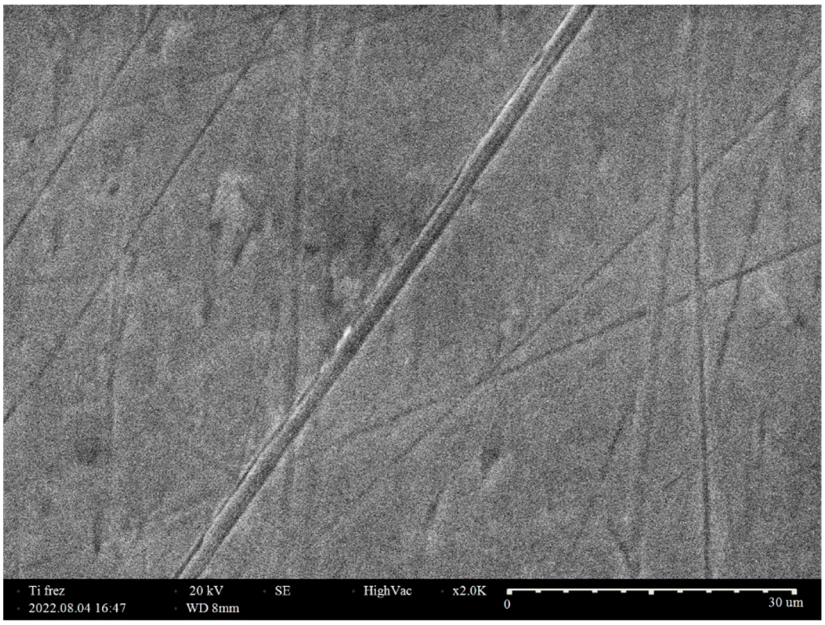

Figure 2. SEM image of the surface of a milled Ti disc specimen marked as Ti frez.

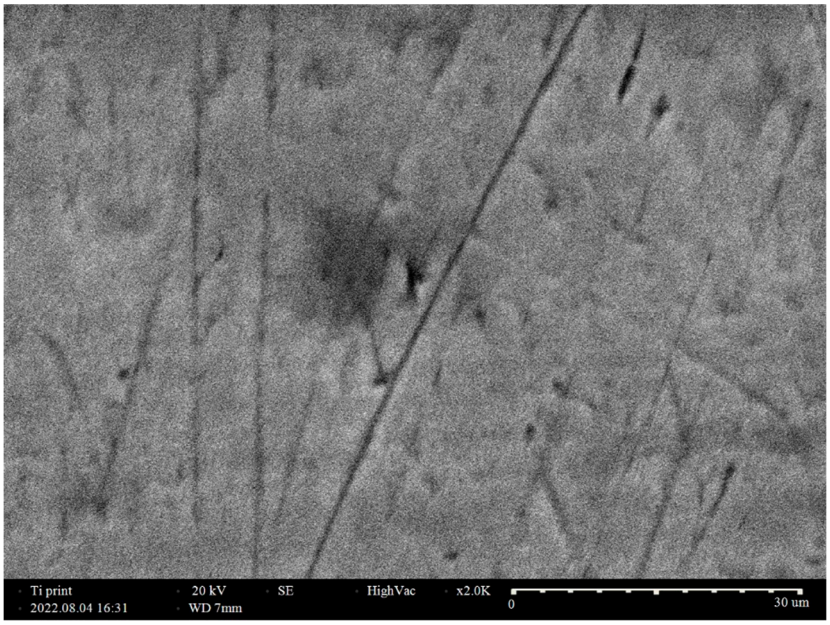

Figure 3. SEM image of the surface of a disk sample of 3D-printed Ti, marked as Ti print.

3.2. XRD results

Investigations were done with a Bruker D8 Advance powder X-ray diffractometer. The Bruker DIFFRAC.EVA program was used to determine the qualitative and quantitative phases of the analysis. Figure 4 shows the diffractogram of the 3D-printed titanium sample. Two phases were found, namely aluminum titanate ($Al_{0.15}Ti_{0.85}$) and less aluminum titanate vanadate (Ti_2VAl). The established hexagonal phase of $Al_{0.15}Ti_{0.85}$ has a crystallite size of 77 nm, and the cubic phase of Ti_2VAl has a crystallite size of 18.5 nm. Figure 5 shows the diffractogram of a milled titanium sample. Two phases were found: mainly aluminum titanate ($Al_{0.15}Ti_{0.85}$) and less titanium vanadate ($Ti_{0.8}V_{0.2}$). A hexagonal phase of $Al_{0.15}Ti_{0.85}$ with crystallite sizes of 106 nm and a cubic phase of $Ti_{0.8}V_{0.2}$ with crystallite sizes of 22.8 nm were found.

Preprints (www.preprints.org) | NOT PEER-REVIEWED | Posted: 10 October 2023 doi:10.20944/preprints202310.0629.v1

The aluminum titanate phase is predominant in both samples, with the differences being a small amount of aluminum titanate vanadate in the printed titanium sample and a small amount of titanium vanadate in the milled titanium sample. With small quantities of chemical elements and compounds in the studied samples and insufficiently manifested peaks, the software detects phases as close to the characteristic peaks from the diffractograms as possible. There was a significant difference in the size of the crystallites of the Al0.15Ti0.85 main phase, with the crystallites (106 nm) in the milled titanium sample being 37% larger than the crystallites in the printed titanium sample (77 nm). For the secondary phases, the milled titanium sample had approximately 20% larger crystallites.

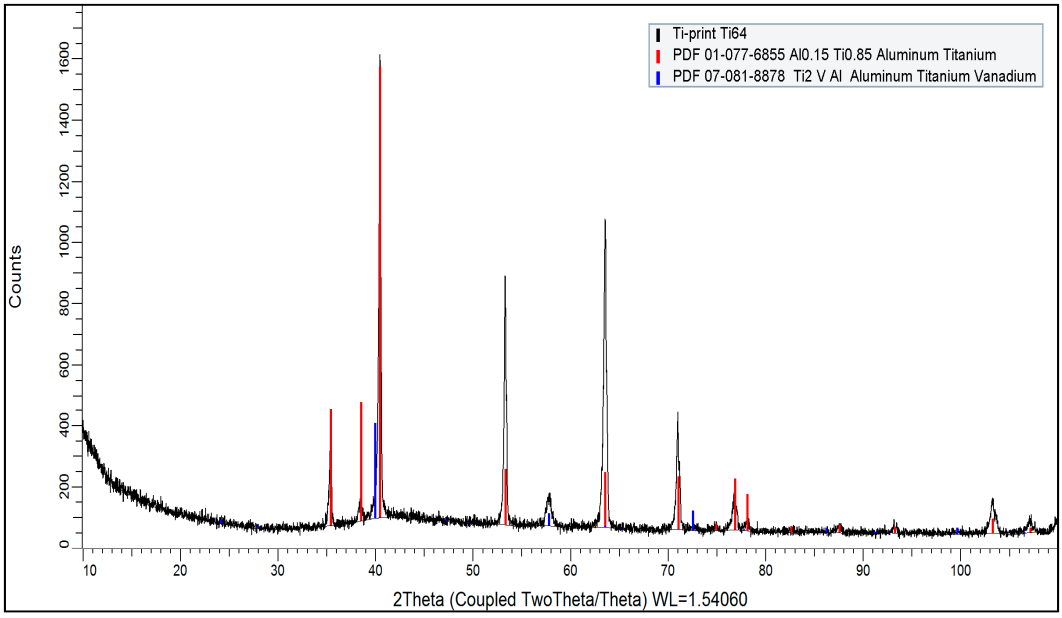

Figure 4. Diffraction pattern of the 3D- printed titanium specimen (Ti-print Ti64).

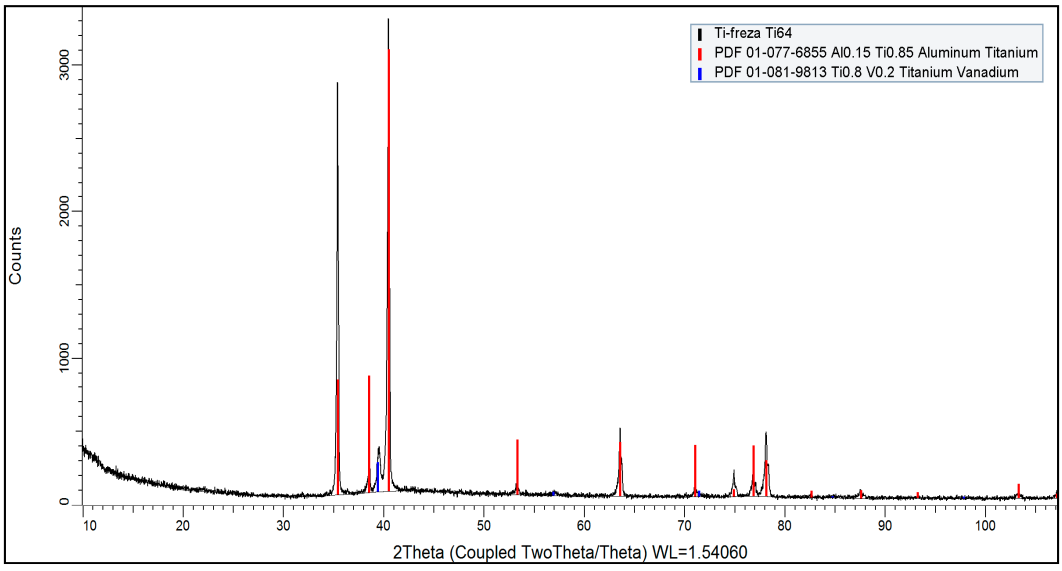

Figure 5. Diffraction pattern of the milled titanium sample (Ti-frez Ti64).

3.3. Nanoindentation results

Load-displacement curves (Figure 6) were obtained as a result of nanoindentation experiments, and the mechanical properties of milled and 3D-printed Ti-6Al-4V samples were calculated using the Oliver & Pharr approximation method [16]. The comparison of indentation hardness H_{IT} and indentation modulus E_{IT} obtained by two production methods of titanium alloys is shown on Figure

Preprints (www.preprints.org) | NOT PEER-REVIEWED | Posted: 10 October 2023 doi:10.20944/preprints202310.0629.v1

7 and Figure 8. The changes of indentation hardness and indentation modulus with depth of indentation were investigated as well, using the cycling indentation method with five loading-unloading cycles.

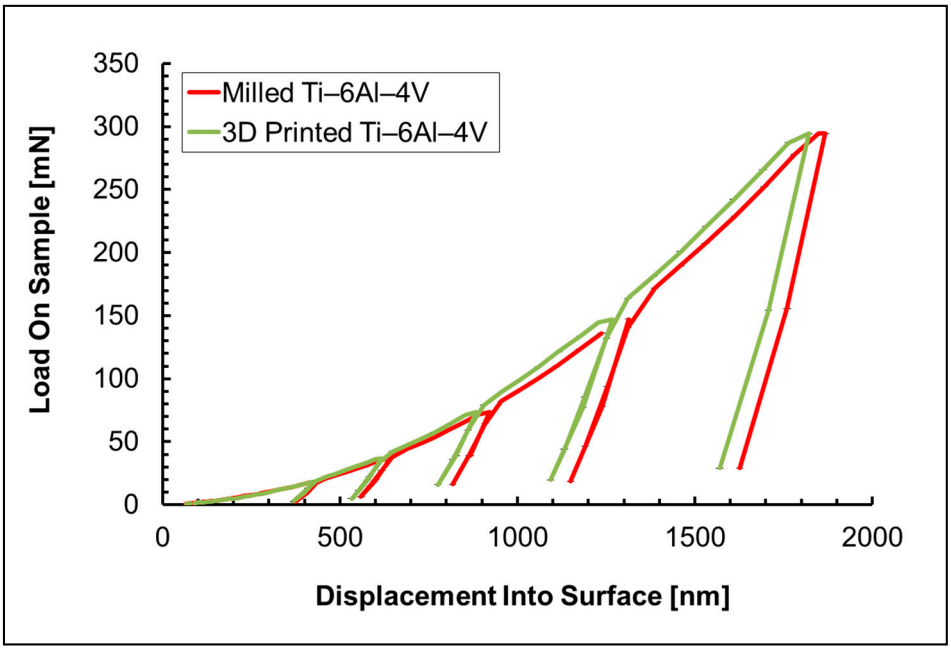

Figure 6. Experimental load-displacement curves.

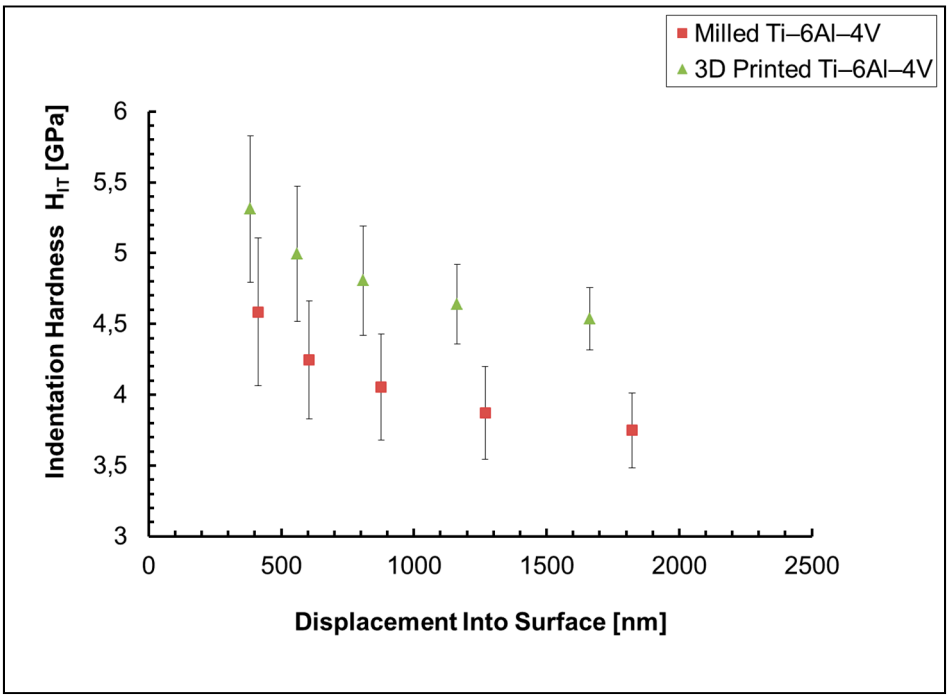

Figure 7. Comparison of indentation hardness of investigated samples from milled and 3D-printed titanium alloys.

Preprints (www.preprints.org) | NOT PEER-REVIEWED | Posted: 10 October 2023 doi:10.20944/preprints202310.0629.v1

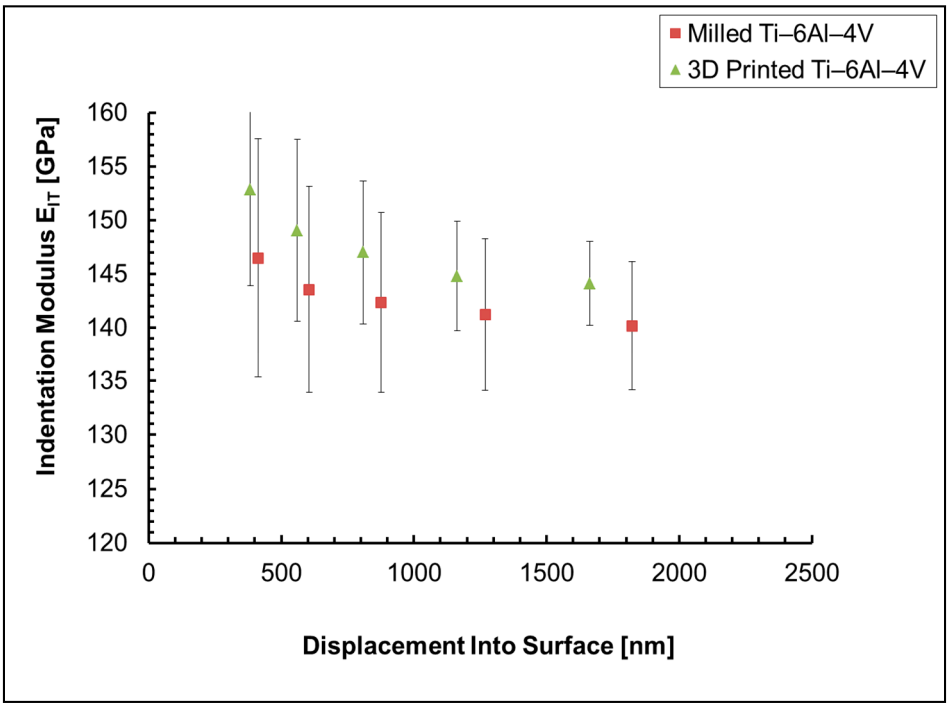

Figure 8. Comparison of indentation modulus of investigated samples from milled and 3D-printed titanium alloys.

3.4. Tensile test results

The stress-strain curves from the tensile test in Figure 9 show significant differences in the behaviour of the studied materials. The curves were calculated and constructed from the immediate data of the machine strain gauge cell. A series of microscopic photographs was taken with a Leica S-6 optical microscope (Germany) of the areas with maximum tensile stresses or the fracture profiles (Figures 10 and 11) of the specimens in order to see their destruction in more detail. A close look at an area close to the fracture site (Figure 10) clearly highlights the disruption of the characteristic surface pattern by machining. This is an unequivocal sign of the plastic deformation of the material. It is expressed in a visible loss of surface flatness and a reduction in cross-sectional area due to the necking process. From a mechanical point of view, this is the occurrence of significant deformation with negligible stress variation, as confirmed by the curve for milled Ti-6Al-4V in Figure 8 in the interval 13–22% of relative deformation.

The fracture profile of the material processed by the SLM technology looks completely different (Figure 11). It can be seen from Figure 9 that the 3D-printed titanium sample does not have such a large flow of plastic deformation. This can explain the characteristic profile of the fracture shown in Figure 11. The comparison of the fracture profile in Figure 11 with that in Figure 10 shows a transitivity of effects from ductile to brittle failure. This trend in the qualities of the materials is also confirmed by the types of curves in Figure 10. An additional feature of the observed areas in Figure 11 (compared to the object in Figure 10) is also the lack of undulation of the surface, characteristic of cases of significant creep of the metal polycrystalline grains.

The obtained by means of a tensile test mechanical properties of the investigated titanium alloys are summarized in Table 2. The color marking of the types of material is for the sake of an easier comparison with the curves in Figure 9. The relative elongation (%) indicated in the table refers to the moment of the maximum strength value reached, and not to the moment of failure of the test specimen.

Preprints (www.preprints.org) | NOT PEER-REVIEWED | Posted: 10 October 2023 doi:10.20944/preprints202310.0629.v1

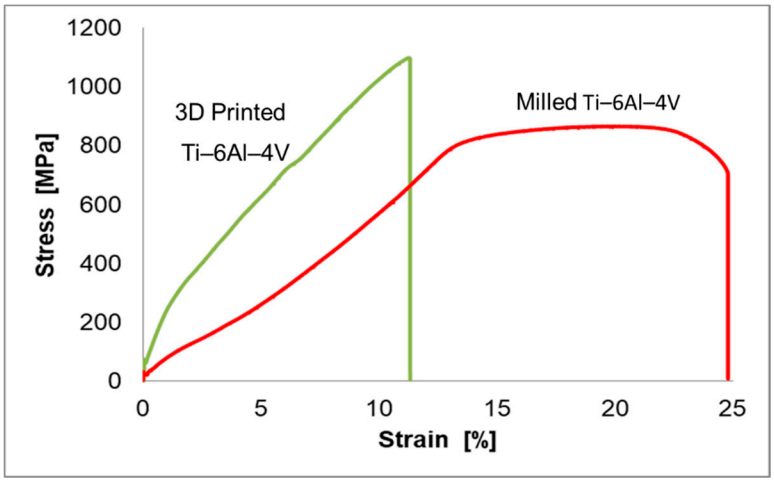

Figure 9. Comparison of the experimental stress-strain curves for 3D printed and milled Ti-6Al-4V samples, obtained by means of tensile test.

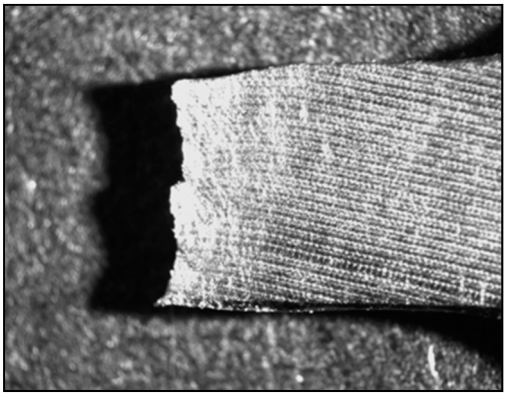

Figure 10. Part of the working area of a milled Ti–6Al–4V specimen (x20) at the point of failure after tensile test.

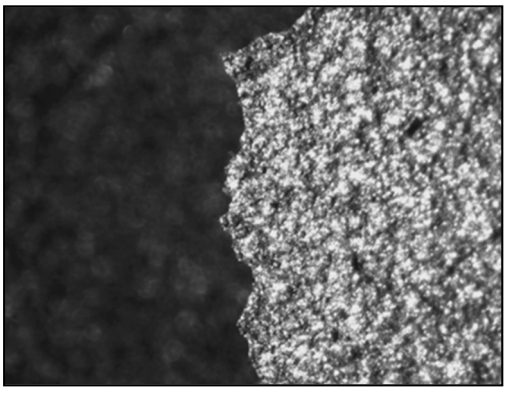

Figure 11. Fracture profile of 3D printed Ti–6Al–4V specimens (x40) after tensile test.

Table 2. The mechanical properties of the alloys established by a tensile test.

No	Material	G^t_{max} [MPa]	$\varepsilon(G^t_{max})$[1] [%]	G^t_{yield} [MPa]	E^t [GPa]
1	Milled Ti-6Al-4V	866	19.5	803.3	7.6
2	3D printed Ti-6Al-4V	1098	11.3	591.8	32.8

[1] G^t_{max} - the maximum tensile stress; $\varepsilon\ (G^t_{max})^1$ - the elongation at the corresponding stress; G^t_{yeld} - tensile stress at 0.2% relative elongation of the specimen; E^t - the tensile modulus of elasticity.

Preprints (www.preprints.org) | NOT PEER-REVIEWED | Posted: 10 October 2023 doi:10.20944/preprints202310.0629.v1

3.5. Bending test results

A bending test by its physical nature involves both tensile and compressive loading. This is a common case in dental medical practice, which justifies the research of materials and constructions based on this method. The outcomes of such tests on the aforementioned materials are summarized in Figure 12. What is immediately noticeable in Figure 12 is that with both types of materials at the initial moments of loading, an unstable development of the load-displacement curve is observed. However, in the initial section, the angular dependence coefficient is analogous to that observed after about 0.5 mm sag of the specimen, which is taken as the region of linear development of the force-displacement curve. From the curves in Figure 12 it is also seen that the milled Ti specimens have a larger plastic strain region than the 3D printed ones. After the load was stopped (at a sag of ~4.9 mm), the 3D-printed Ti specimens showed cracks in the region of maximum tensile stresses.

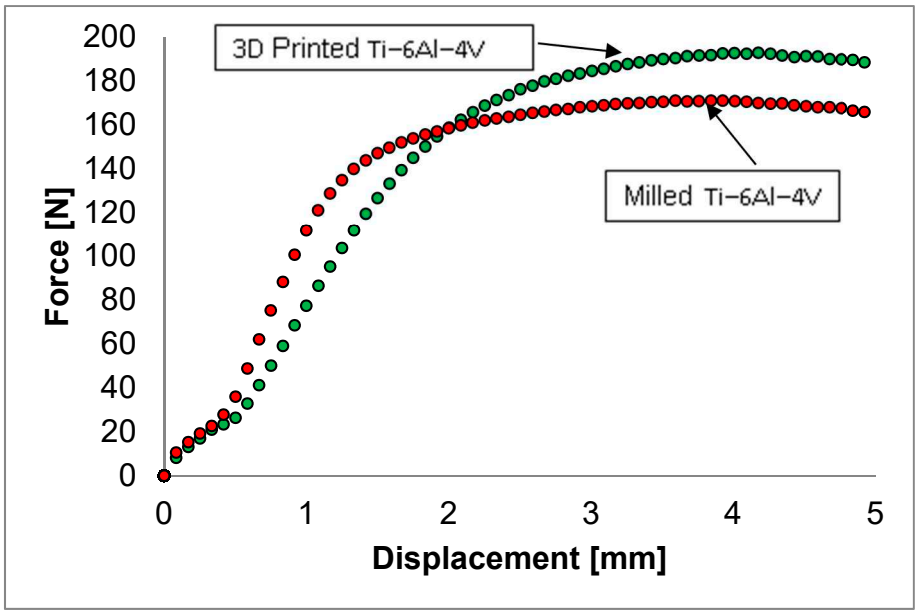

Figure 12. Load-displacement curves, obtained by means of 3-point bending test (1 mm/min).

Confirmation of the assumption about the different ability of the studied materials to develop plastic deformation can be seen in the pictures from the optical microscope in Figure 13 and Figure 14. Those areas of the test specimens that have sustained the greatest tensile stress are shown there. An additional possibility was to check for the existence of a possible influence of the different strain rates. Upon careful comparison of the two pictures ((a) and (b)) in Figure 13, a violation of the specific texture of the surface of the object in Figure 13(b) can be noticed. This is due to the creep effect of the material, the analogue of which was observed in Figure 10. It is important to note that the strain rate did not lead to the appearance of visible cracks.

The result of the same deformation impact on the 3D-printed Ti-6Al-4V test specimens is significantly different. In order to better highlight the difference caused by the loading speed, the side view of the test specimens was chosen (Figure 14).

In contrast to the mechanical processing of the surfaces, with the "SLM" technology, surfaces with a granular structure are obtained. In this sense, the natural lack of sufficient smoothness of the walls of the test specimens does not allow the sharp distinction of the edge from the adjacent walls of the specimen. This is the reason for the questionable accuracy when measuring the depth of the formed crack. A consequence of this is the impossibility of assessing the degree of influence of the loading rate. It is important to note that at the same degree of deformation, we observe consecutive plastic deformation processes and, subsequently, the appearance of a crack. Because of the degree of deformation realized, no moment of final separation of the specimen into two parts was reached, regardless of the bending speed. The results of the three-point bending test are summarized in Table

Preprints (www.preprints.org) | NOT PEER-REVIEWED | Posted: 10 October 2023 doi:10.20944/preprints202310.0629.v1

3. The color marking of the materials is for the sake of an easier comparison with the curves in Figure 12. The sample with second indices "2" was tested at an indenter displacement speed of 60 mm/min.

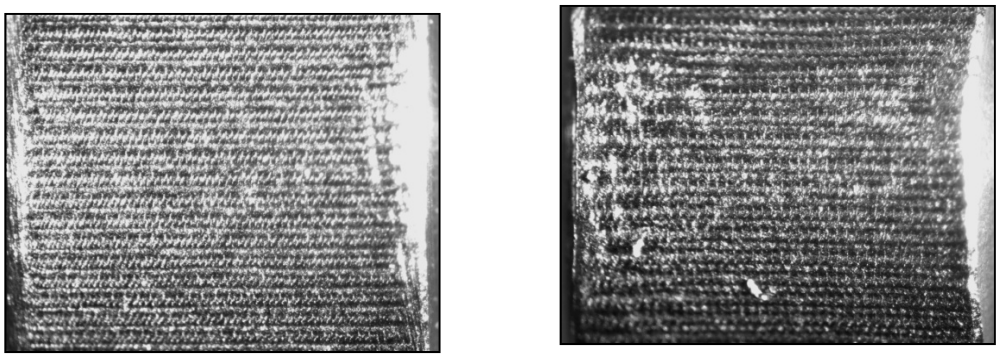

(a) (b)

Figure 13. Frontal view in the region of the realized maximum tensile stress of milled Ti specimens at different indenter movement speeds: (a) 1 mm/min /x40/; (b) 60mm/min /x40/.

(a) (b)

Figure 14. Side view in the area of the realized maximum tensile-compressive stress of 3D printed Ti-6Al-4V specimens at different indenter movement speeds: (a) 1 mm/min /x35/; (b) 60 mm/min /x35.

Table 3. Flexural strength (classical method) of the tested materials.

No	Material	G^f [GPa]	E^f [GPa]
1.1	Milled Ti	1639	97
1.2	Milled Ti	1719	99
2.1	3D printed Ti-6Al-4V	1997	78

G^f - the maximum bending stress; E^f - flexural modulus of elasticity.

3.6. AFM results

The topography and surface roughness of the samples were investigated using atomic force microscope. AFM's high-resolution imaging capability enables the precise location of indentation positions and their depth measurement [17].The applied roughness analysis of each AFM image uses R_a, R_q and R_{max} values calculated according to the relative heights of each pixel of the topography of the studied sample [18].

The roughness analysis gives the value R_a which is the arithmetic mean of the absolute values Z_j of the surface height deviations measured from the mean plane

$$R_a = \frac{1}{n}\sum_{j=1}^{N}|Z_j| \ , \quad (1)$$

while R_q is the root-mean-square value of the height deviations taken from the plane of the average image data [18].

Preprints (www.preprints.org) | NOT PEER-REVIEWED | Posted: 10 October 2023 doi:10.20944/preprints202310.0629.v1

$$R_q = \sqrt{\frac{\sum_{j=1}^{N} z_j^2}{N}} \quad (2)$$

The AFM images of milled and 3D-printed Ti-6Al-4V samples were compared and presented in Figure 15. The morphology of the milled Ti-6Al-4V sample with a scanning area of 10×10 μm² (Figure 15 (a)) reveals a rougher surface in comparison with the morphology of the 3D-printed Ti-6Al-4V sample with the same scan area (Figure 15 (b)), which is smoother with a homogeneous structure. The measured roughness of the milled Ti-6Al-4V sample for R_q is 15.2 nm, and for the value of R_a it is 12.0 nm. On the other hand, the roughness of the 3D-printed Ti-6Al-4V sample for R_q is 10.9 nm, and for the value of R_a it is 8.65 nm, respectively.

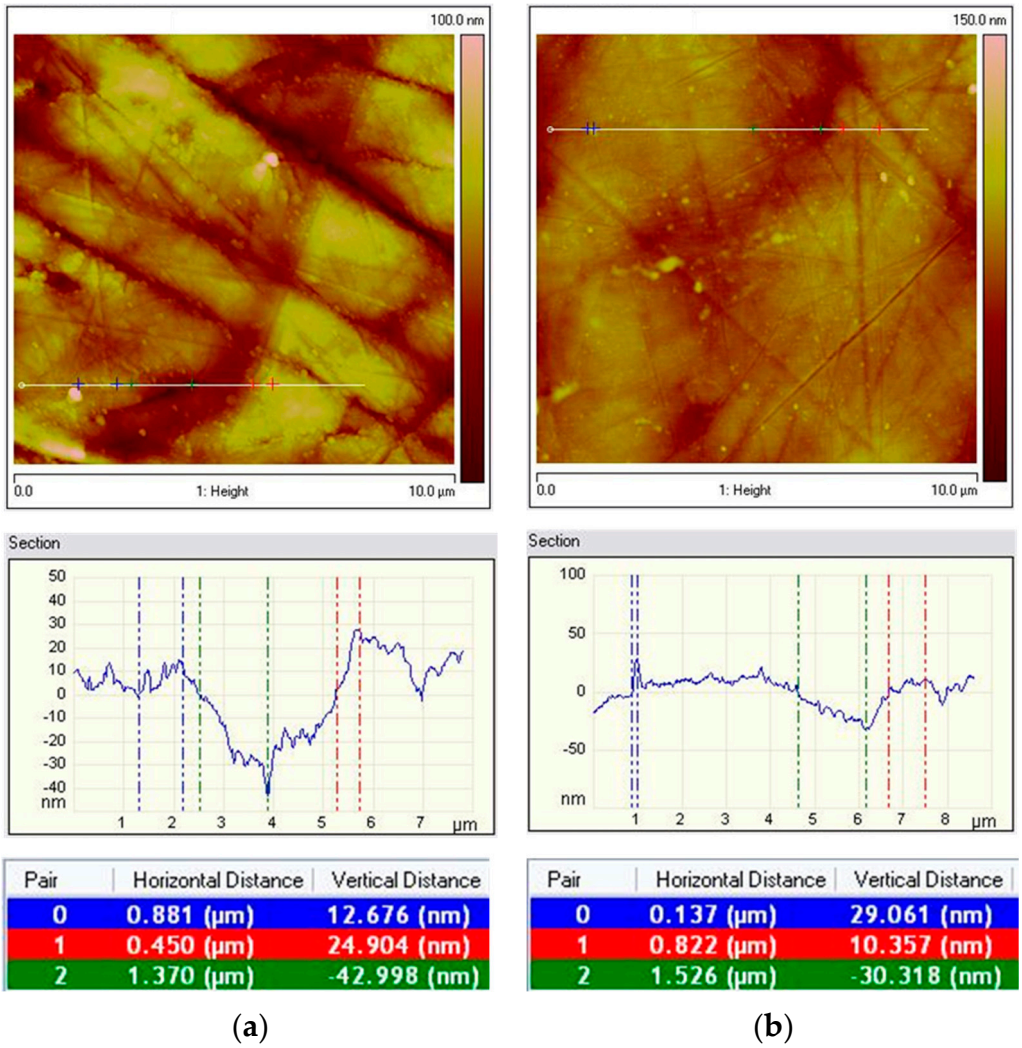

Figure 15. AFM topography of the samples: Milled Ti-6Al-4V (a) and 3D Printed Ti-6Al-4V (b): 2D images and section analysis.

For a better evaluation of the morphology of the two samples, 2D and 3D images of milled Ti-6Al-4V and 3D-printed Ti-6Al-4V samples were compared with a scanning area of 5×5 μm² (Figure 16). The images show that the 3D-printed Ti-6Al-4V sample has a smooth surface with the presence of small nanometric spheres. The milled Ti-6Al-4V sample, on the other hand, has a rough surface with larger and smaller clusters.

Preprints (www.preprints.org) | NOT PEER-REVIEWED | Posted: 10 October 2023 doi:10.20944/preprints202310.0629.v1

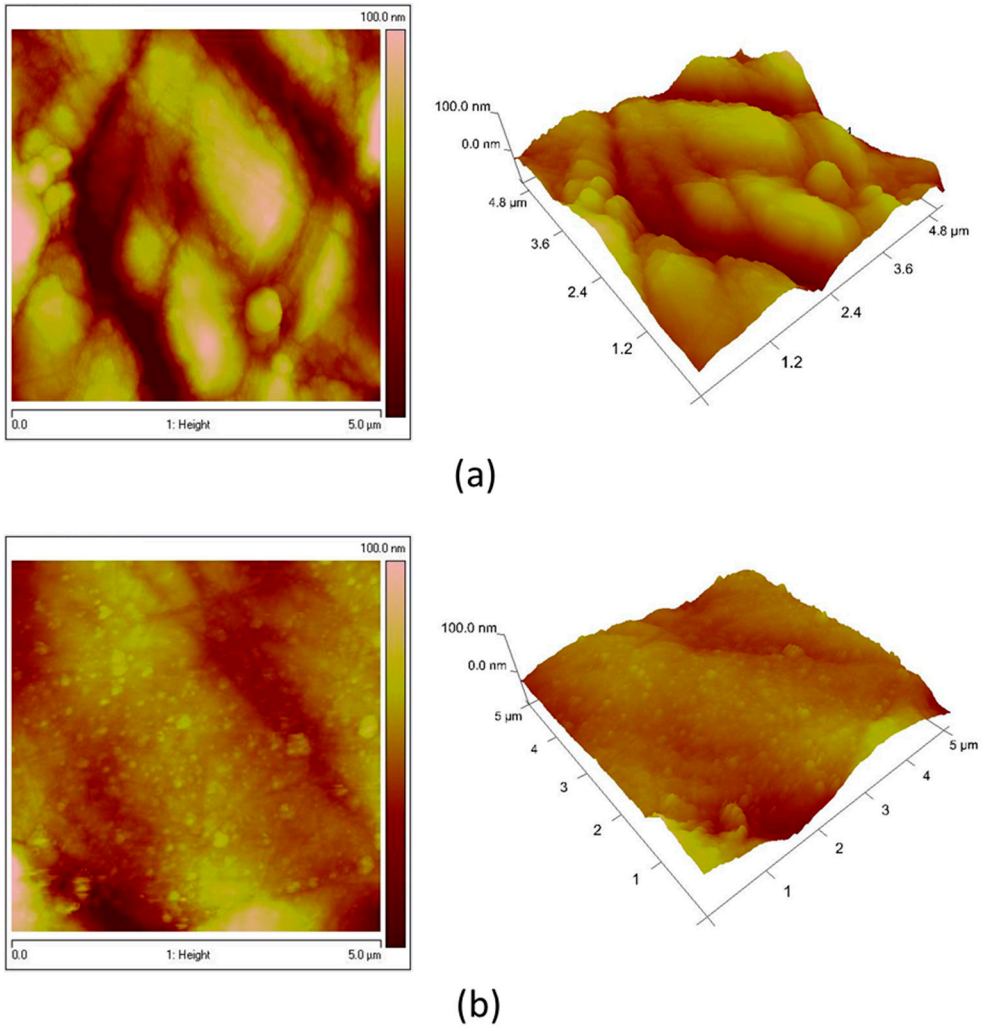

Figure 16. 2D and 3D AFM images of the samples: Milled Ti-6Al-4V (a) and 3D Printed Ti-6Al-4V (b).

3.7. Statistical comparisons

In the 3D-printed Ti-6Al-4V sample, the indentation modulus individual values ranged from 138.69 GPa to 153.87 GPa, and in the milled Ti-6Al-4V sample, the range spanned from 128.024 GPa to 155.22 GPa. The mean value was 3.97 GPa higher in the 3D-printed Ti-6Al-4V sample than in the milled Ti-6Al-4V sample, with a statistically significant difference ($p = 0.009$).

The individual indentation hardness varied from 4.12 GPa to 4.85 GPa in the 3D-printed Ti-6Al-4V specimens and from 3.21 GPa to 4.42 GPa in the milled Ti-6Al-4V specimens. The mean indentation hardness was 0.79 GPa higher in the 3D-printed Ti-6Al-4V sample as compared to the milled Ti-6Al-4V sample, $p < 0.001$ (Table 4).

Table 4. Results from the t-test comparison of the 3D-printed Ti-6Al-4V sample with the milled Ti-6Al-4V sample.

Parameters	Mean	SD	Mean difference	95% CI difference		p-value
				Lower	Upper	
Indentation modulus						
o 3D printed Ti-6Al-4V	144.12	3.89	3.97	1.03 to 6.90		0.009

Preprints (www.preprints.org) | NOT PEER-REVIEWED | Posted: 10 October 2023 doi:10.20944/preprints202310.0629.v1

○ Milled Ti 6Al-4V	140.15	5.98			
Indentation hardness					
○ 3D printed Ti-6Al-4V	4.53	0.22			
○ Milled Ti 6Al-4V	3.74	0.26	0.79	0.64 to 0.93	<0.001

4. Discussion

The nanoindentation experiments revealed significant differences in indentation modulus and indentation hardness between the 3D-printed Ti-6Al-4V specimens and the milled Ti-6Al-4V specimens. Both parameters had higher values in the 3D-printed Ti-6Al-4V sample. One reason for this result is that the 3D-printed Ti-6Al-4V sample had smaller crystallite sizes than the milled one. The same tendency was obtained for Young's modulus of both samples, obtained by means of the tensile test (Table 2), but the values were smaller than those of the indentation modulus. This is because the indentation modulus is calculated in some sample volume, while the Young's modulus is calculated in some direction [19]. The obtained results for indentation hardness are in agreement with those obtained by Peng [20]. At the same time, it was found that as indentation depth increased, the indentation hardness and modulus of both titanium alloys decreased slightly. For the milled Ti, Titan BioStar Grade 5 discs (SILADENT Dr. Böhme & Schöps GmbH) were used in the production process. According to the certificate provided by the manufacturer Siladent [21], the chemical composition of the titanium discs used for production of the milled sample is as follows: 88% Ti, 6.75% Al, 4.5% V, <1% others (N; C; H; Fe; O).

According to the certificate provided by the manufacturer Carpenter Technology [22], of the powder used for production of the 3D-printed sample, the chemical composition of the metal powder PowderRange Ti64 is as follows: ~89% Ti, Aluminum 5.50–6.50 %, Vanadium 3.50–4.50 %, Iron 0.25 %, Oxygen 0.13 %, Carbon 0.08 %, Nitrogen 0.03 %, Hydrogen 0.0125 %, Yttrium 0.005 %, Other, each < 0.10 %, Other, total < 0.40 %. The slightly higher concentration of titanium in the composition, as well as the slightly lower concentration of aluminum, could be another reason for the higher indentation hardness obtained with the 3D-printed titanium sample.

The results from the tensile test showed that the 3D-printed sample made by means of selective laser melting (SLM) technology had about 26% higher tensile strength and smaller elongation than the milled one. The same tendency for yield strength and elongation was obtained by Karolewska and Ligaj [23].

The results from the 3-point bending test showed that the 3D-printed Ti-6Al-4V sample had higher flexural strength than the milled one. Two different strain rates (1 mm/min and 60 mm/min) were used, and their influence on the obtained flexural strength was investigated as well. The strength achieved at different loading rates may be a function of the manufacturing method of the test specimens. For the milled Ti-6Al-4V specimens, increasing speed causes a proportional increase in recorded strength of ~4.9%.

As the roughness of the sample surface can have an influence on the nanoindentation results, AFM was used to study the surface topography and roughness of both titanium alloys. The AFM observation of the surface topography of the investigated samples showed that the milled Ti-6Al-4V sample was characterized by a higher roughness than the 3D-printed one.

From a clinical perspective, the higher modulus of elasticity as well as tensile and flexural strengths of printed titanium make it suitable for the fabrication of larger prosthetic structures, especially implant-supported ones. Its smoother surface is an advantage when polishing, especially on areas in contact with soft tissues.

When Ti G5 is used to make orthodontic retainers, milled titanium is more suitable. It has lower indentation hardness and indentation modulus, which would allow, with the same parameters as

printed Ti, greater individual tooth mobility in the retention period of teeth fixed with a retainer. Its rougher surface is a disadvantage that can be removed with the subsequent processing of the metal.

5. Conclusions

The structure, morphology and mechanical properties of two titanium alloys, produced by two different methods (milled and 3D printed by means of selective laser melting) were investigated and compared. Tensile test, a three-point bending test, nanoindentation, and atomic force microscopy were used for determination of mechanical properties and surface roughness of investigated titanium alloys. The results showed that the 3D-printed Ti-6Al-4V sample has higher indentation hardness, indentation modulus, tensile strength, flexural strength, and smaller roughness than the milled one.

The structure and morphology of the samples were investigated by means of SEM and XRD. A significant difference in the size of the crystallites of the $Al_{0.15}Ti_{0.85}$ main phase was observed; in the milled titanium sample, the crystallites were 37% larger than the crystallites of the printed titanium sample. For the secondary phases, approximately 20% larger crystallites were observed in the milled titanium sample. According to the Hall-Petch relationship [24] smaller crystallite size of the 3D-printed sample could be one of the reasons for its higher indentation hardness. From a clinical point of view, despite the differences in the mechanical properties of milled and printed Ti, both metals are sufficient for the loads they can be subjected to in the oral cavity. According to the clinical situation and the specifics of the construction for which it will be used, it is a matter of judgment which type of titanium will be selected.

Author Contributions: Conceptualization, V.P.; methodology, S.Ch. and V.P.; formal analysis, S.Ch. and V.P; investigation, S.Ch., V.P., V.B., S.S.; resources, V.P.; data curation, V.B.; writing—original draft preparation, S. Ch.; writing—review and editing, V.P.; visualization, S.S, V.B and V.P; supervision, S.Ch. and V.P..; project administration, S.Ch..; funding acquisition, S.Ch.. All authors have read and agreed to the published version of the manuscript."

Funding: The APC was funded by the Operational Program of EU "Science and Education for Smart Growth" under grant number BG05M2OP001-1.001- 0008.

Data Availability Statement: The data presented in this study are available on request from the corresponding author.

Conflicts of Interest: The authors declare no conflict of interest.

References

1. Alghazzawi, T. F. Advancements in CAD/CAM technology: Options for practical implementation. *J Prosthodont Res* **2016**, 60, 72- 84.
2. Arnold, C.; Hey, J.; Schweyen, R.; Setz, J.M. Accuracy of CAD/CAM fabricated removable partial dentures. *J Prosthet Dent* **2018,** *119*, 586-590.
3. Shannon, T.; Groth, C. Be your own manufacturer: 3D printing intraoral appliances. *Semin Orthod* **2021,** *27*, 184–188.
4. Alshhrani, W.; Al Amri, M. Customized CAD/CAM healing abutment for delayed loaded implants. *J Prosthet Dent* **2016**, *116*,176-179.
5. Skjerven, H.; Riis, U.; Herlofsson, B.; Ellingsen, J. In vivo accuracy of implant placement using a full digital planning modality and stereolithographic guides. *Int J Oral Maxillofac Impl* **2019,** *34*, 124–132.
6. Sriram, S; Shankari, V.; Chacko, Y. Computer Aided Designing/Computer Aided Manufacturing in Dentistry (CAD/ CAM) – A Review. *Int J Cur Res Rev* **2018**, *10*, 21- 24.
7. Ortorp, A.; Jonsson, D.; Mouhsen, A.; Vult von Steyern, P. The fit of cobalt-chromium three-unit fixed dental prostheses fabricated with four different techniques: a comparative in vitro study. *Dent Mat* **2011,** *27*, 356–363.
8. Abele, E.; Frohlich, B. High speed milling of titanium alloys. *Adv Prod Eng & Manag* **2008**, *3*, 131–140.
9. ISO/ASTM 52900:2015 (ASTM F2792). Additive manufacturing- general principles and terminology. Available online: https://www.iso.org/ standard/69669.html?browse=tc. (accessed on 6 October 2023).
10. Atzeni, E.; Salmi, A. Economics of additive manufacturing for end-usable metal parts. *Int. J Adv Manuf Technol* **2012,** *62*, 1147–1155.
11. Zheng, Q.; Mao, L.; Shi, Y.; Fu, W.; Hu, Y. Biocompatibility of Ti-6Al-4V titanium alloy implants with laser microgrooved surfaces. *Mat Techn* **2022,** *37*, 2039-2048.

12. Sidambe, A. Biocompatibility of Advanced Manufactured Titanium Implants—A Review. *Materials* **2014,** *7*, 8168-8188.
13. Elias, C.; Fernandes, D.; de Souza, F.; Monteiro, E.; de Biasi, R. Mechanical and clinical properties of titanium and titanium-based alloys (Ti G2, Ti G4 cold worked nanostructured and Ti G5) for biomedical applications. *J Mater Res Technol* **2019,** *8*, 1060-1069.
14. Belan, J.; Kucharikova, L.; Tillova, E.; Chalupov, M. Three-Point Bending Fatigue Test of TiAl6V4 Titanium Alloy at Room Temperature. *Adv Mater Sci Engin* **2019**, 2842416.
15. ISO 14577-1:2015 Metallic materials — Instrumented indentation test for hardness and materials parameters — Part 1: Test method
16. Oliver, W.C.; Pharr, G.M. An improved technique for determining hardness and elastic modulus using load and displacement sensing indentation experiments. *J Mater Res* **1992,** *7*, 1564–1583.
17. Jalili, H.; Laxminarayana, K.A. Review of atomic force microscopy imaging systems: application to molecular metrology and biological sciences. *Mechatronics* **2004,** *14*, 907-945.
18. Eaton, P.; West, P. *Atomic Force Microscopy*, 1st ed.; OXFORD University Press Inc.: New York, USA, 2010.
19. Chudoba, T. Measurement of Hardness and Young's Modulus by Nanoindentation. In *Nanostructured Coatings. Nanostructure Science and Technology,* 1st ed;. Cavaleiro, A., De Hosson, J.T.M., Eds.; Springer: New York, USA, 2006; pp. 216-260.
20. Peng, H.; Fang, W.; Dong, C.; Yi, Y.; Wei, X.; Luo, B.; Huang, S. Nano-Mechanical Properties and Creep Behavior of Ti6Al4V Fabricated by Powder Bed Fusion Electron Beam Additive Manufacturing. *Materials* **2021,** *14*, 3004.
21. Titan BioStar Grade 5(Siladent). Available online: https://www.siladent-shop.de/sicherheitsdb_en/128260_TITAN_BioStar.pdf (accessed on 6 October 2023).
22. Powder Range Ti64 datasheet (Carpenter Additive). Available online: https:// www.carpenteradditive.com/hubfs/Resources/Data%20Sheets/PowderRange_TI64_Datasheet.pdf (accessed on 6 October 2023).
23. Karolewska, K.; Ligaj, B. Comparison Analysis of Titanium Alloy Ti6Al4V Produced by Metallurgical and 3D Printing Method. *AIP Conf Proc* **2019,** *2077,* 020025-1- 020025-8.
24. Smith, W.F.; Hashemi, J. *Foundations of Materials Science and Engineering,* 4th ed.; McGraw-Hill; New York, USA, 2006.